

# Strain penetration of high-strength steel bars anchored in reinforced concrete beam-column connections

Ling Li<sup>1</sup>, Wenzhong Zheng<sup>\*1,2,3</sup> and Ying Wang<sup>1</sup>

<sup>1</sup>School of Civil Engineering, Harbin Institute of Technology, Harbin 150090, China;

<sup>2</sup>Key Lab of Structures Dynamic Behaviour and Control of the Ministry of Education, Harbin Institute of Technology, Harbin 150090, China

<sup>3</sup>Key Lab Smart Prevention and Mitigation of Civil Engineering Disasters of the Ministry of Industry and Information Technology, Harbin Institute of Technology, Harbin 150090, China

(Received July 23, 2018, Revised August 4, 2019, Accepted August 27, 2019)

**Abstract.** This paper presents experimental and analytical investigations on additional fixed-end rotations resulting from the strain penetration of high-strength reinforcement in reinforced concrete (RC) beam-column connections under monotonic loading. The experimental part included the test of 18 interior beam-column connections with straight long steel bars and 24 exterior beam-column connections with hooked and headed steel bars. Rebar strains along the anchorage length were recorded at the yielding and ultimate states. Furthermore, a numerical program was developed to study the effect of strain penetration in beam-column connections. The numerical results showed good agreement with the test results. Finally, 87 simulated specimens were designed with various parameters based on the test specimens. The effect of concrete compressive strength ( $f_c$ ), yield strength ( $f_y$ ), diameter ( $d_b$ ), and anchorage length ( $l_{ah}$ ) of the reinforcement in the beam-column connection was examined through a parametric study. The results indicated that additional fixed-end rotations increased with a decrease in  $f_c$  and an increase in  $f_y$ ,  $d_b$  and  $l_{ah}$ . Moreover, the growth rate of additional fixed-end rotations at the yielding state was faster than that at the ultimate state when high-strength steel bars were used.

**Keywords:** reinforced concrete; bond-slip; strain penetration; numerical analysis; fixed-end rotation

## 1. Introduction

In reinforced concrete (RC) frame structures, plastic hinges are generally designed to form at the beam end of the beam-column connections based on the principle of strong column and weak beam. As the maximum moment occurs at the beam-column interface, a concrete crack develops at this section and the tensile force is sustained by the steel bars alone. The rebar stress at the critical section is transmitted along the anchorage length in beam-column connections because of the bond between reinforcement and concrete. Hence, rebar strains gradually decrease over the anchorage length, which is referred to as strain penetration of longitudinal reinforcement. A slip of reinforcement occurs at the beam-column interface due to the accumulation of the rebar strains along the anchorage length. This slip is different from the one due to bond failure and will result in an additional fixed-end rotation, which in turn affects the rotation of the plastic hinge in the frame beam.

To account for the influence of additional fixed-end rotation on the plastic hinge, models for an equivalent plastic hinge length that incorporate strain penetration effects were proposed (Paulay and Prestley 1992,

Panagiotakos and Fardis 2001). The contribution of strain penetration was commonly considered as a linear function of  $(f_y d_b)$ , where  $f_y$  and  $d_b$  denote the yield strength and diameter of the reinforcement. In this way, it is convenient to determine the additional fixed-end rotation due to strain penetration. Nevertheless, other parameters that play an important role in strain penetration effects have not been fully considered. Therefore, an attempt has been made in this study to comprehensively and quantitatively investigate the parameters affecting additional fixed-end rotation, including the yield strength and diameter of high-strength reinforcement, concrete compressive strength, ratio of neutral axis depth to section effective depth, and straight lead anchorage length in the beam-column connection.

To investigate strain penetration of the anchorage reinforcement, many theoretical and experimental studies have been conducted with columns, walls and beam-column connections (Saatcioglu *et al.* 1992, Monti *et al.* 1997, Sezen and Moehle 2003, Mergos 2012, Mergos 2013, Alva 2013, Mergos and Kappos 2016). As the strain penetration effects of reinforcements are obvious when subjected to tension and compression alternately, most of these RC members were tested or simulated under cyclic loading. However, with an increase in the yield strength of steel bars specified in the current design standards, degradation of the local bond between the concrete and reinforcement is accelerated. Under these conditions, the strain penetration of high-strength anchorage reinforcement in RC members

\*Corresponding author, Ph.D., Professor  
E-mail: zhengwenzhonghit@163.com

Table 1 Reinforcement details in the specimens

Series	Specimens No.	Concrete grade	Longitudinal reinforcement in beams				
			Grade	Top	Bottom	Anchorage type	$l_{ah}$ (mm)
I	IA-400-C40-18	C40		3 $\Phi$ 18	2 $\Phi$ 10		400
	IA-400-C50-18	C50		3 $\Phi$ 18	2 $\Phi$ 10		400
	IA-400-C60-18	C60		3 $\Phi$ 18	2 $\Phi$ 10		400
	IA-600-C40-20	C40		2 $\Phi$ 20	2 $\Phi$ 10		600
	IA-600-C50-20	C50	HRB500	2 $\Phi$ 20	2 $\Phi$ 10	straight	600
	IA-600-C60-20	C60		2 $\Phi$ 20	2 $\Phi$ 10		600
	IA-800-C40-22	C40		2 $\Phi$ 22	2 $\Phi$ 10		800
	IA-800-C50-22	C50		2 $\Phi$ 22	2 $\Phi$ 10		800
	IA-800-C60-22	C60		2 $\Phi$ 22	2 $\Phi$ 10		800
	IB-400-C40-18	C40		3 $\Phi$ 18	2 $\Phi$ 10		400
	IB-400-C50-18	C50		3 $\Phi$ 18	2 $\Phi$ 10		400
	IB-400-C60-18	C60		3 $\Phi$ 18	2 $\Phi$ 10		400
	IB-600-C40-20	C40		2 $\Phi$ 20	2 $\Phi$ 10		600
	IB-600-C50-20	C50	HRB600	2 $\Phi$ 20	2 $\Phi$ 10	straight	600
	IB-600-C60-20	C60		2 $\Phi$ 20	2 $\Phi$ 10		600
	IB-800-C40-22	C40		2 $\Phi$ 22	2 $\Phi$ 10		800
	IB-800-C50-22	C50		2 $\Phi$ 22	2 $\Phi$ 10		800
	IB-800-C60-22	C60		2 $\Phi$ 22	2 $\Phi$ 10		800
E	EA-430-C40-18	C40		3 $\Phi$ 18	2 $\Phi$ 10	straight	430
	EA-380-C50-18	C50		3 $\Phi$ 18	2 $\Phi$ 10	straight	380
	EA-350-C60-18	C60		3 $\Phi$ 18	2 $\Phi$ 10	straight	350
	EA-330-C40-20	C40		2 $\Phi$ 20	2 $\Phi$ 10	hooked	330
	EAH-190-C40-20	C40		2 $\Phi$ 20	2 $\Phi$ 10	headed	190
	EA-420-C50-20	C50	HRB500	3 $\Phi$ 20	2 $\Phi$ 10	straight	420
	EA-300-C50-20	C50		3 $\Phi$ 20	2 $\Phi$ 10	hooked	300
	EAH-270-C60-20	C60		3 $\Phi$ 20	2 $\Phi$ 10	headed	270
	EA-160-C60-20	C60		3 $\Phi$ 20	2 $\Phi$ 10	hooked	160
	EA-210-C40-22	C40		2 $\Phi$ 22	2 $\Phi$ 10	hooked	210
	EA-190-C50-22	C50		2 $\Phi$ 22	2 $\Phi$ 10	hooked	190
	EA-300-C60-22	C60		2 $\Phi$ 22	2 $\Phi$ 10	hooked	300
	EB-420-C40-18	C40		3 $\Phi$ 18	2 $\Phi$ 10	straight	420
	EB-420-C50-18	C50		3 $\Phi$ 18	2 $\Phi$ 10	straight	420
	EB-400-C60-18	C60		3 $\Phi$ 18	2 $\Phi$ 10	straight	400
	EB-380-C40-20	C40		2 $\Phi$ 20	2 $\Phi$ 10	hooked	380
	EBH-220-C40-20	C40		2 $\Phi$ 20	2 $\Phi$ 10	headed	220
	EB-420-C50-20	C50	HRB600	2 $\Phi$ 20	2 $\Phi$ 10	straight	420
	EB-340-C50-20	C50		2 $\Phi$ 20	2 $\Phi$ 10	hooked	340
	EBH-310-C60-20	C60		2 $\Phi$ 20	2 $\Phi$ 10	headed	310
EB-180-C60-20	C60		2 $\Phi$ 20	2 $\Phi$ 10	hooked	180	
EB-230-C40-22	C40		2 $\Phi$ 22	2 $\Phi$ 10	hooked	230	
EB-210-C50-22	C50		2 $\Phi$ 22	2 $\Phi$ 10	hooked	210	
EB-340-C60-22	C60		2 $\Phi$ 22	2 $\Phi$ 10	hooked	340	

Note: 1.  $\Phi$ ,  $\Phi$ ,  $\Phi$  and  $\Phi$  respectively indicate reinforcement grades of HPB300, HRB400, HRB500 and HRB600;  
2. Letter H in the 'specimens No.' indicates the headed reinforcement embedded in the beam-column connection.

under monotonic loads becomes more prominent. Therefore, a combination of experimental study and numerical analysis is employed in the current study to investigate additional fixed-end rotations due to strain penetration of high-strength reinforcement in RC beam-column connections under monotonic loads.

In the slight of the above, 18 interior beam-column connections with high-strength straight long reinforcement and 24 exterior beam-column connections with high-strength hooked and headed reinforcement were tested under monotonic loading in this paper. We are focused on the additional fixed-end rotation at the yielding state (rebar strain at the critical section reaches yield strain) and ultimate state (concrete strain in the extreme compressed fibre of the critical section reaches ultimate strain). Furthermore, numerical analysis was conducted to study strain penetration of the reinforcement in the test specimens. A parametric study on 87 beam-column connections, which were designed based on the test specimens, was performed to investigate the factors influencing strain penetration of reinforcement. The main objective of this study is to provide better insights into the variations of additional fixed-end rotation with respect to the main influence parameters, which may serve as a basis for RC structure design.

## 2. Experimental program

### 2.1 Specimen details

A total of 42 RC specimens were designed and tested to study strain penetration of the tensile steel bars anchored in beam-column connections. The specimens consisted of a cantilever beam, middle column, and bottom beam. The function of the bottom beams was to connect the beam-column connections to the ground so as to maintain their stability in the process of loading. The reinforcement details in the specimens are listed in Table 1.

The specimens, designed based on strong column-weak beam requirements, were divided into two types to model the interior beam-column connections (series I) and exterior beam-column connections (series E) of a RC building structure, respectively. Four control variables were considered in the design, namely, the yield strength  $f_y$  and diameter  $d_b$  of the tensile reinforcement, concrete compressive strength  $f_c$ , and the straight lead anchorage length  $l_{ah}$  of the tensile reinforcement in the beam-column connection. A consistent coding system was used to label the specimens. A typical example of such coding is IA-400-C40-18, where "I" indicates the specimen series and "A" indicates the grade of tensile reinforcement (A and B represent HRB500 and HRB600 steel bars, respectively). The subsequent number "400" represents the straight anchorage length of the tensile reinforcement in the beam-column connection (unit: mm). The third part C40 indicates the concrete grade (the concrete grade in this study contains C40, C50 and C60 as per the Chinese code GB 50010-2010), and the last number "18" represents the diameter of the tensile reinforcement (unit: mm).

Table 2 Material properties of concrete

Grade	C40	C50	C60
Cubic strength $f_{cu}$ (MPa)	50.6	59.2	74.3
Compressive strength $f_c$ (MPa)	40.5	47.4	61.9

Note: For concrete below C50 grade, the compressive strength  $f_c$  was calculated as 0.8 times the cubic strength  $f_{cu}$ , the compressive strength  $f_c$  of C60 concrete was calculated as  $0.833f_{cu}$ .

Table 3 Material properties of reinforcement

Grade	Diameter (mm)	Yield strength $f_y$ (MPa)	Ultimate strength $f_u$ (MPa)	Yield strain $\epsilon_y$	Percentage elongation at maximum force $\epsilon_u$
HPB300	10	381	513	0.00191	0.150
HRB400	10	498	632	0.00249	0.148
	18	460	621	0.00230	0.136
HRB500	18	590	749	0.00295	0.112
	20	581	732	0.00291	0.122
	22	543	713	0.00272	0.113
HRB600	18	631	825	0.00316	0.108
	20	654	837	0.00327	0.104
	22	628	801	0.00314	0.107

Table 2 lists the properties of the concrete. The cubic strength of concrete  $f_{cu}$  was calculated using cubes with a side of 150 mm and they were prepared and cured in the same manner as the test specimens. The deformed steel bars were tested under uniaxial tension and the values of the obtained parameters are listed in Table 3.

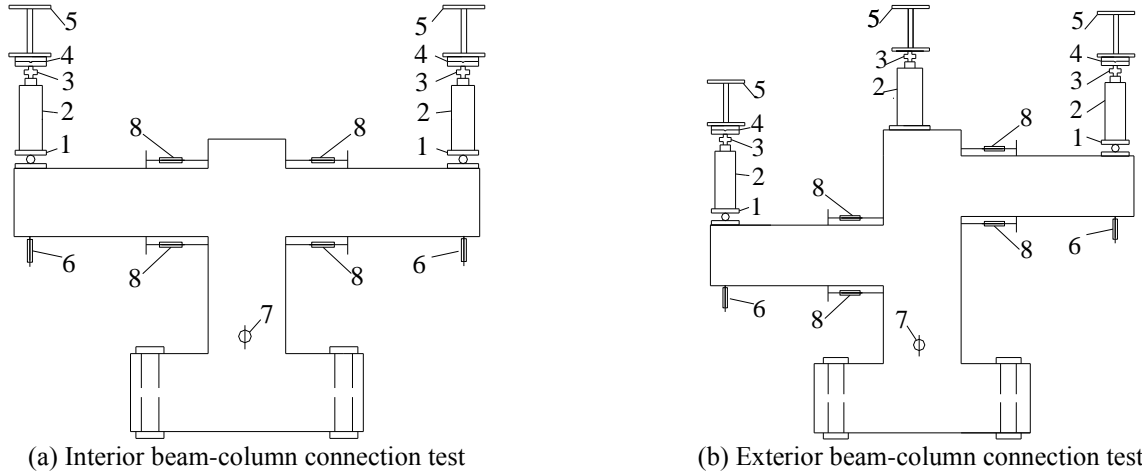
### 2.2 Test scheme

A point monotonic load was applied symmetrically using two loading jacks at the end of the cantilever beams, as shown in Fig. 1. The applied load was measured by the sensors placed on each loading jack. Strain gauges with a width of 1 mm and length of 2 mm were attached to the steel bars along the straight anchorage length in the beam-column connections.

The spacing between the strain gauges was 40 mm. To obtain the rebar strain accurately, the strain gauges were attached in the notch of the reinforcement, which was slotted adjacent to the longitudinal ribs, as shown in Fig. 2. Such placement can minimize the losses of the bonding performance of the tensile longitudinal reinforcement to a significant extent. Fig. 3 shows the locations of the strain gauges.

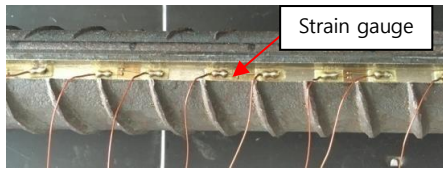
## 3. Numerical program

A numerical program was developed to study strain penetration of the reinforcement in beam-column connections. The stress state of the anchorage reinforcement and bonded concrete is complicated. In this study, we attempted to simplify it into a one-dimensional problem.

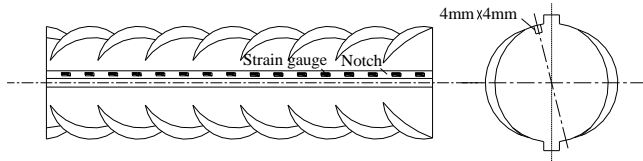


1. Rolling hinge support; 2. Loading jack; 3. Loading sensor; 4. Blade hinge support; 5. Trestle; 6. Displacement transducers; 7. Dial indicator; 8. Extensometer.

Fig. 1 Test rigs and instrumentations



(a) Slotting on steel bars



(b) Schematic diagram

Fig. 2 Strain gauges attached along the notch

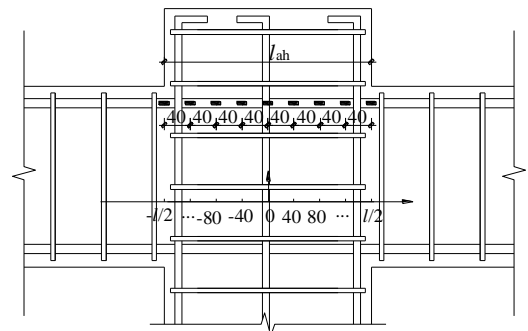
### 3.1 Material constitutive law

In the case of concrete, the stress-strain relationship follows CEB-FIP Model Code 2010, as shown in Fig.4, and the corresponding equations are:

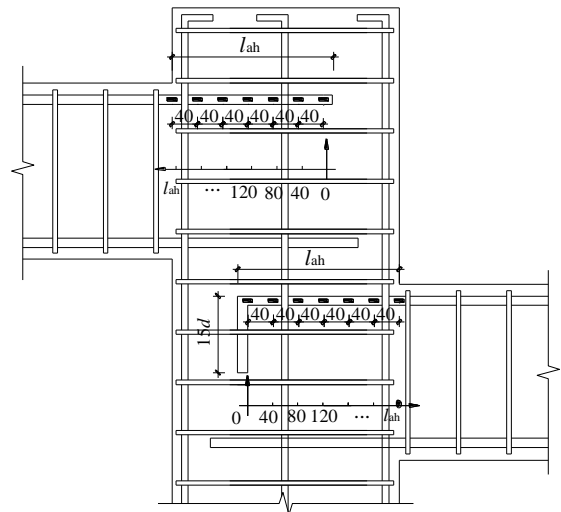
$$\frac{\sigma_c}{f_c} = -\frac{k \cdot \frac{\varepsilon_c}{\varepsilon_{c1}} - (\frac{\varepsilon_c}{\varepsilon_{c1}})^2}{1 + (k-2) \frac{\varepsilon_c}{\varepsilon_{c1}}} \quad \text{for } |\varepsilon_c| < |\varepsilon_{c,lim}| \quad (1)$$

$$\sigma_{ct} = \begin{cases} E_{ci} \cdot \varepsilon_{ct} & \text{for } \sigma_{ct} \leq 0.9f_{ct} \\ \varepsilon_{ct} \cdot (1 - 0.1 \frac{1.5 \times 10^{-4} - \varepsilon_{ct}}{1.5 \times 10^{-4} - 0.9 \cdot \frac{\varepsilon_{ct}}{E_{ci}}}) & \text{for } 0.9f_{ct} \leq \sigma_{ct} \leq f_{ct} \end{cases} \quad (2)$$

where  $\sigma_c$  and  $\varepsilon_c$  are the stress and strain of compression concrete,  $\varepsilon_{c,lim}$  is the ultimate compressive strain,  $f_c$  is the concrete compressive strength,  $\varepsilon_{c1}(\%) = -0.7f_c^{0.31}$  is the strain at maximum compressive stress,  $k = -1.1E_c \cdot (\varepsilon_c/f_c)$  is the plasticity number, and  $E_c = 22 \cdot (f_c/10)^{0.3}$ .  $\sigma_{ct}$  and  $\varepsilon_{ct}$  represent the stress and strain of tensile concrete,  $f_{ct}$  is the tensile strength of concrete, and  $E_{ci}$  is the elastic modulus of concrete at the age of 28 days.



(a) Interior beam-column connection



(b) Exterior beam-column connection

Fig. 3 Configuration of strain gauges

The bilinear stress-strain relationship, which considers strain hardening, was used to model tensile steel bars, as shown in Fig.5, and can be represented by Eq.(3)

$$\begin{aligned} \sigma_s &= E_s \varepsilon_s & \text{for } 0 \leq \varepsilon_s \leq \varepsilon_{sy} \\ \sigma_s &= f_y + E_{sh}(\varepsilon_s - \varepsilon_{sy}) & \text{for } \varepsilon_s > \varepsilon_{sy} \end{aligned} \quad (3)$$

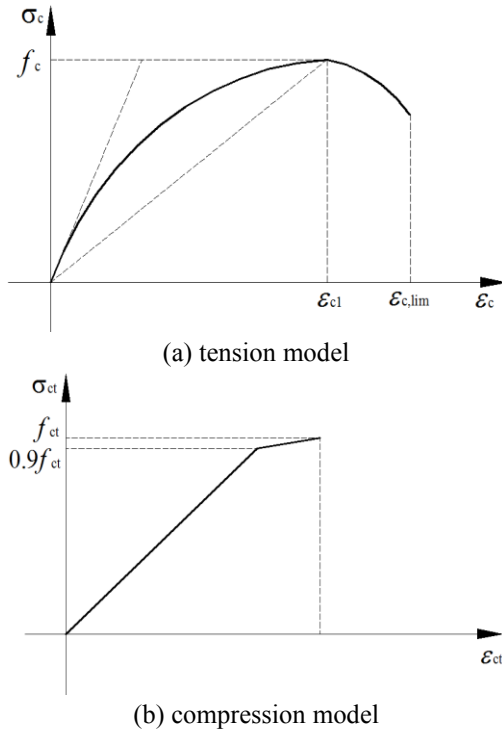


Fig.4 Stress-strain relationship of concrete

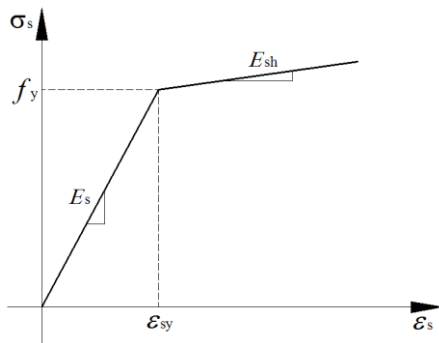


Fig. 5 Stress-strain relationship of steel bars

where  $\sigma_s$  and  $\varepsilon_s$  are the stress and strain of the tensile steel bar,  $f_y$  is the yield stress,  $\varepsilon_{sy}=f_y/E_s$  is the yield strain,  $E_s$  is the elastic modulus of steel bars, which is taken as 200 GPa, and  $E_{sh}$  is the hardening modulus of reinforcement, normally assumed to be 0–0.05 GPa.

The 4-segment curve of bond stress-slip relationship between concrete and steel bars, specified by CEB-FIP Model Code 2010, was adopted in this investigation, as shown in Fig.6. It can be defined using the following expressions:

$$\begin{aligned} \tau &= \tau_{\max} \left(\frac{s}{s_1}\right)^\alpha && \text{for } 0 \leq s \leq s_1 \\ \tau &= \tau_{\max} && \text{for } s_1 < s \leq s_2 \\ \tau &= \tau_{\max} - (\tau_{\max} - \tau_f) \left(\frac{s-s_2}{s_3-s_2}\right) && \text{for } s_2 < s \leq s_3 \\ \tau &= \tau_f && \text{for } s_3 < s \end{aligned} \quad (4)$$

where  $\tau$  and  $s$  are the bond and slip between concrete and

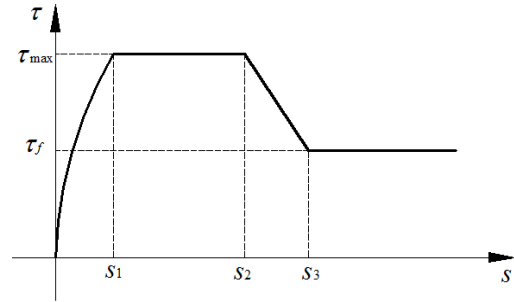


Fig. 6 Bond-slip relationship between concrete and reinforcement

reinforcement,  $\tau_{\max} = 1.25\sqrt{f_c}$  is the maximum bond stress, and  $\tau_f = 0.4\tau_{\max}$  is the residual bond stress. According to CEB-FIP Model Code 2010,  $s_1 = 1.8\text{mm}$ ,  $s_2 = 3.6\text{mm}$ ,  $s_3 = c_{\text{clear}}$  ( $c_{\text{clear}}$  is the clear distance between ribs) and  $\alpha = 0.4$ .

### 3.2 Equilibrium equations and boundary conditions

As shown in Fig. 7, the model considering strain penetration of the reinforcement in beam-column connections involves six variables.  $\sigma_s(x)$  and  $\varepsilon_s(x)$  denote the stress and strain of the anchorage reinforcement due to strain penetration, respectively.  $\tau(x)$  is the bond stress between reinforcement and concrete.  $\sigma_c(x)$  and  $\varepsilon_c(x)$  are the stress and strain of the concrete, respectively, resulting from the stress transmitted by  $\tau(x)$ .  $s(x)$  is the relative slip caused by the incoordination between  $\varepsilon_s(x)$  and  $\varepsilon_c(x)$ .

An infinitesimal element of length  $dx$  was considered along the anchorage length and force analysis corresponding to this element is shown in Fig. 7. Fig. 7(b) shows the stress condition of the infinitesimal element for anchored reinforcement. In this case, the equilibrium of the steel bar in the infinitesimal element can be written as Eq.(5):

$$\tau(x) + \frac{d_b}{4} \cdot \frac{d\sigma_s}{dx} = 0 \quad (5)$$

Fig. 7(c) shows the stress and strain conditions of the steel bar and concrete. Displacement compatibility equation between the reinforcement and concrete is given by Eq.(6):

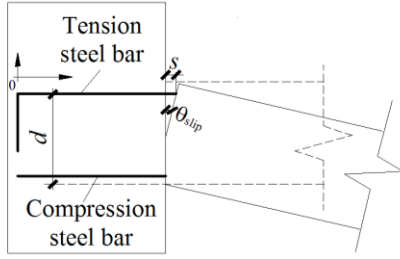
$$ds = (\varepsilon_s - \varepsilon_c)dx \quad (6)$$

Fig. 7(d) shows the force condition of the RC element and its equilibrium equation can be obtained using the following equation:

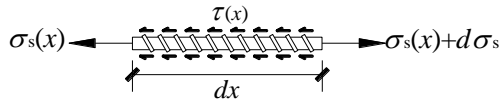
$$\frac{\pi d_b^2}{4} \cdot d\sigma_s + A_c d\sigma_c = 0 \quad (7)$$

where  $d_b$  is the diameter of the steel bar, and  $A_c$  is the area of tensile cord.

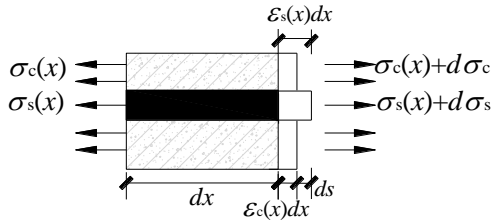
At the yielding and ultimate states, a concrete crack develops at the beam-column interface, where the tensile stress in concrete is zero. Rebar strain at the beam-column interface can be obtained from the internal force balance of the cross section. Thus, the boundary conditions at the beam-column interface can be summarized as follows



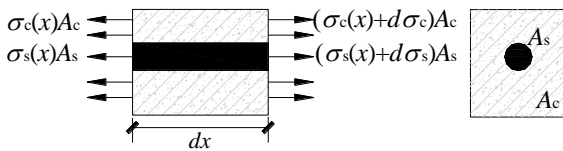
(a) additional fixed-end rotation at beam- column interface



(b) stress acting on a steel bar element



(c) stress and strain of a reinforced concrete element



(d) force acting on a reinforced concrete element

Fig. 7 Model of strain penetration in beam-column connections

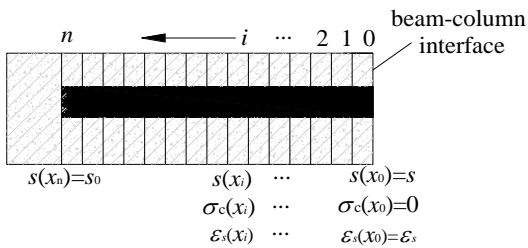


Fig. 8 Division of the units and direction of the recursive calculation

$$\sigma_c(x=0) = 0 \tag{8}$$

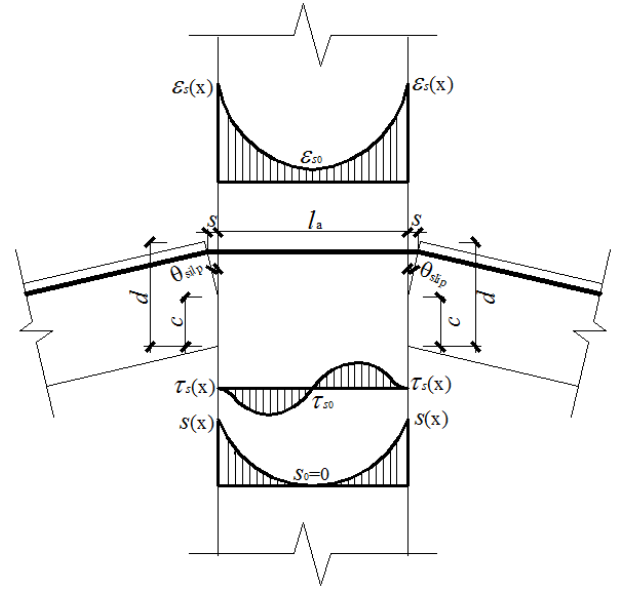
$$\epsilon_s(x=0) = \epsilon_{sy} \text{ or } \epsilon_{su} \tag{9}$$

$$s(x=0) = s_{0,y} \text{ or } s_{0,u} \tag{10}$$

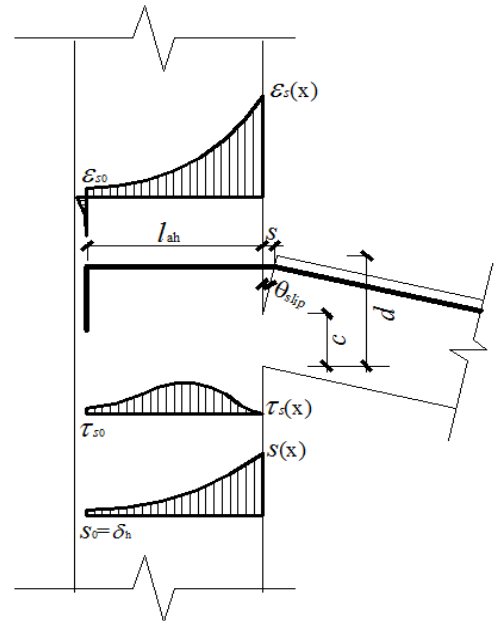
where  $\epsilon_{sy}$  and  $\epsilon_{su}$  are the rebar strain at yielding and ultimate states,  $s_{0,y}$  and  $s_{0,u}$  are the slip at the loaded end of the anchorage reinforcement at yielding and ultimate states, respectively, and  $l_{ah}$  is the straight lead anchorage length.

### 3.3 Analysis program

Fig. 8 shows a straight steel bar anchored in the beam-column connection. The length of the anchorage



(a) interior beam-column connection



(b) exterior beam-column connection

Fig. 9 Strain penetration of the longitudinal tensile reinforcement in beam-column connection

reinforcement is divided into infinitesimal length  $dx$ . Applying an assumed slip  $s$  at the beam-column interface, which may cause the change of the six basic variables for each infinitesimal element. Combining with the material constitutive law given by Eqs. (1)-(4), the six variables mentioned above can be determined by recursive calculation using Eqs. (5)-(7), as described below:

$$\sigma_s(x_{i+1}) = \sigma_s(x_i) - \frac{4\tau(x_i)}{d_b} dx \tag{11}$$

$$\sigma_c(x_{i+1}) = \sigma_c(x_i) - (\sigma_s(x_i) - \sigma_s(x_{i+1})) \frac{A_s}{A_c} \tag{12}$$

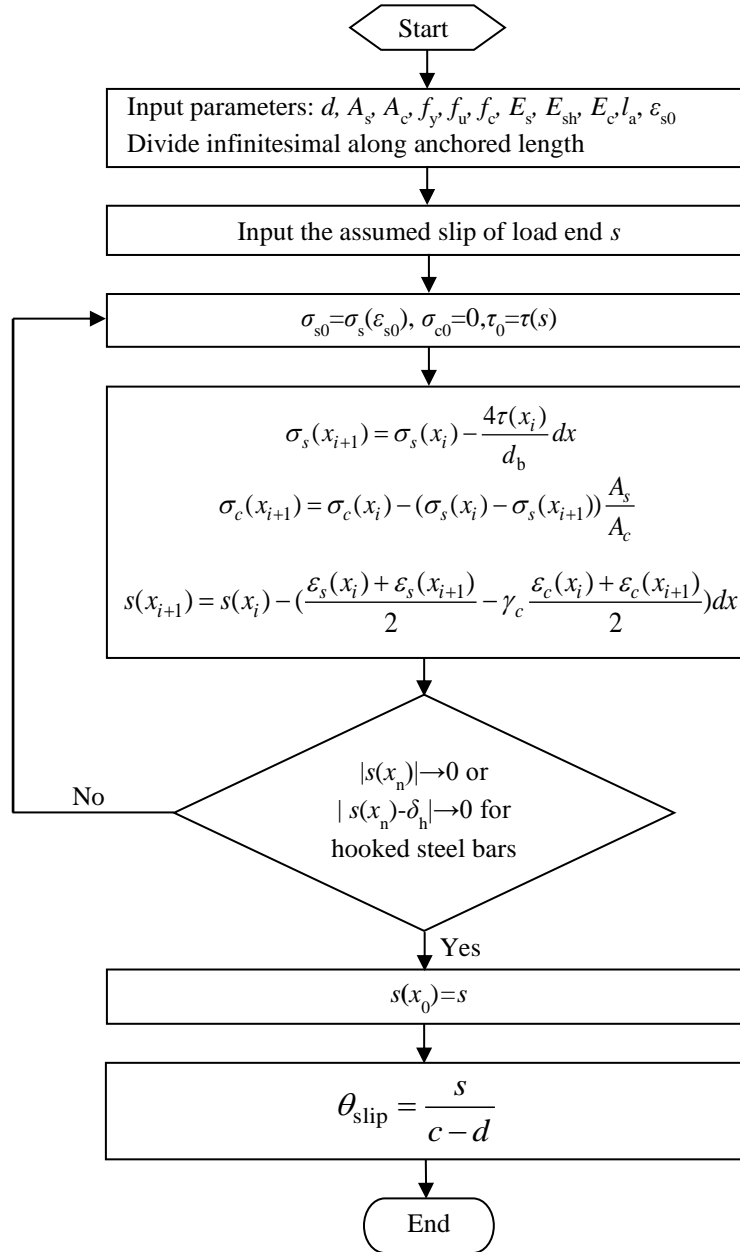


Fig. 10 Flowchart of the numerical analysis program

$$s(x_{i+1}) = s(x_i) - \left( \frac{\epsilon_s(x_i) + \epsilon_s(x_{i+1})}{2} - \gamma_c \frac{\epsilon_c(x_i) + \epsilon_c(x_{i+1})}{2} \right) dx \quad (13)$$

where  $\gamma_c$  denotes the ratio of concrete strain at the reinforcement interface to the cross-sectional concrete strain, and  $\gamma_c = 2.0$  is considered a reasonable value based on test results (Xu *et al.* 1994). Recurrence was stopped until the boundary conditions in Eqs. (8)-(10) were satisfied. Then, distribution of rebar strain  $\epsilon_s(x)$  along the anchorage length was obtained.

Disregarding concrete strain in tension, reinforcement slip at the beam-column interface  $s$  can be calculated by integrating  $\epsilon_s(x)$  along the anchorage length

$$s = \int_0^{l_{ah}} \epsilon_s(x) dx + \delta_h \quad (14)$$

where  $l_{ah}$  is the straight lead length of the steel bars. For the hooked bars embedded in the concrete, when  $l_{ah}$  is not long

enough to sustain the applied force, a hook displacement of  $\delta_h$  occurs. It can be calculated from the model of the relationship between the hook force and hook displacement, based on tensile behavior experiments of the hook bars proposed by Soroushian *et al.* (1988).

Fig. 9(a) and 9(b) illustrate the additional fixed-end rotation  $\theta_{slip}$  at the beam-column interface due to strain penetration of flexural reinforcement inside the interior and exterior beam-column connections.  $\theta_{slip}$  is equal to the slip of anchorage reinforcement  $s$  divided by the depth of the tensile zone ( $d-c$ ), as given by Eq. (15)

$$\theta_{slip} = \frac{s}{d-c} \quad (15)$$

where  $d$  is the effective depth of the section, and  $c$  is the depth of neutral axis. The flowchart of the analysis program for additional fixed-end rotation is shown in Fig. 10.

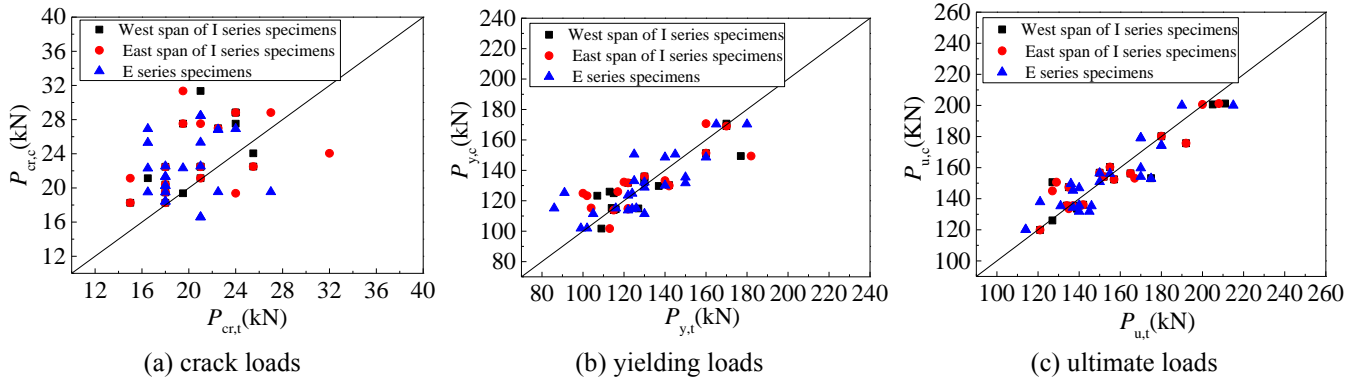


Fig.11 Comparison between experimental loads and numerical calculations

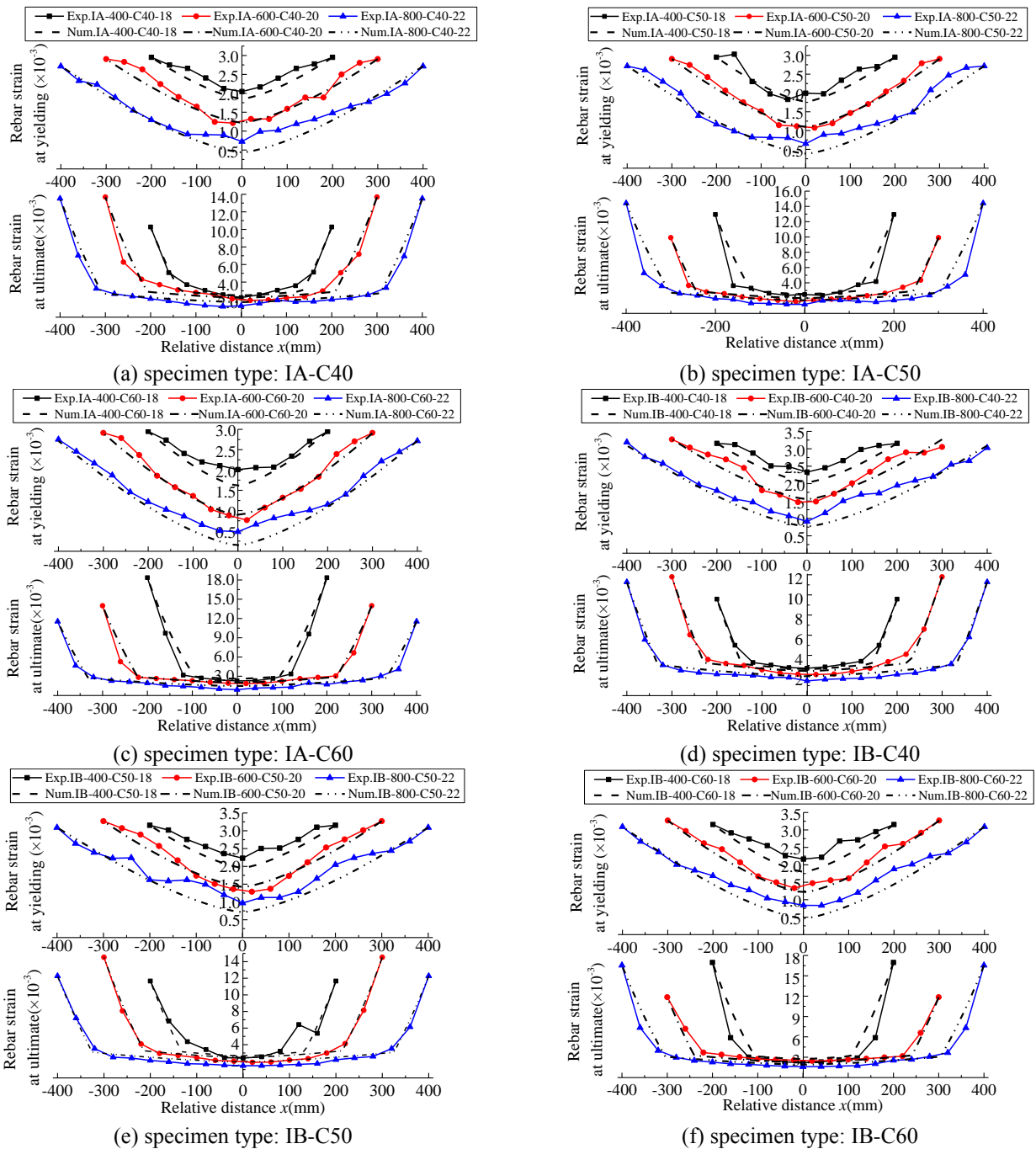


Fig.12 Comparisons between the experimental and numerical results of the rebar strain distribution in the interior beam-column connections at the yielding and ultimate states

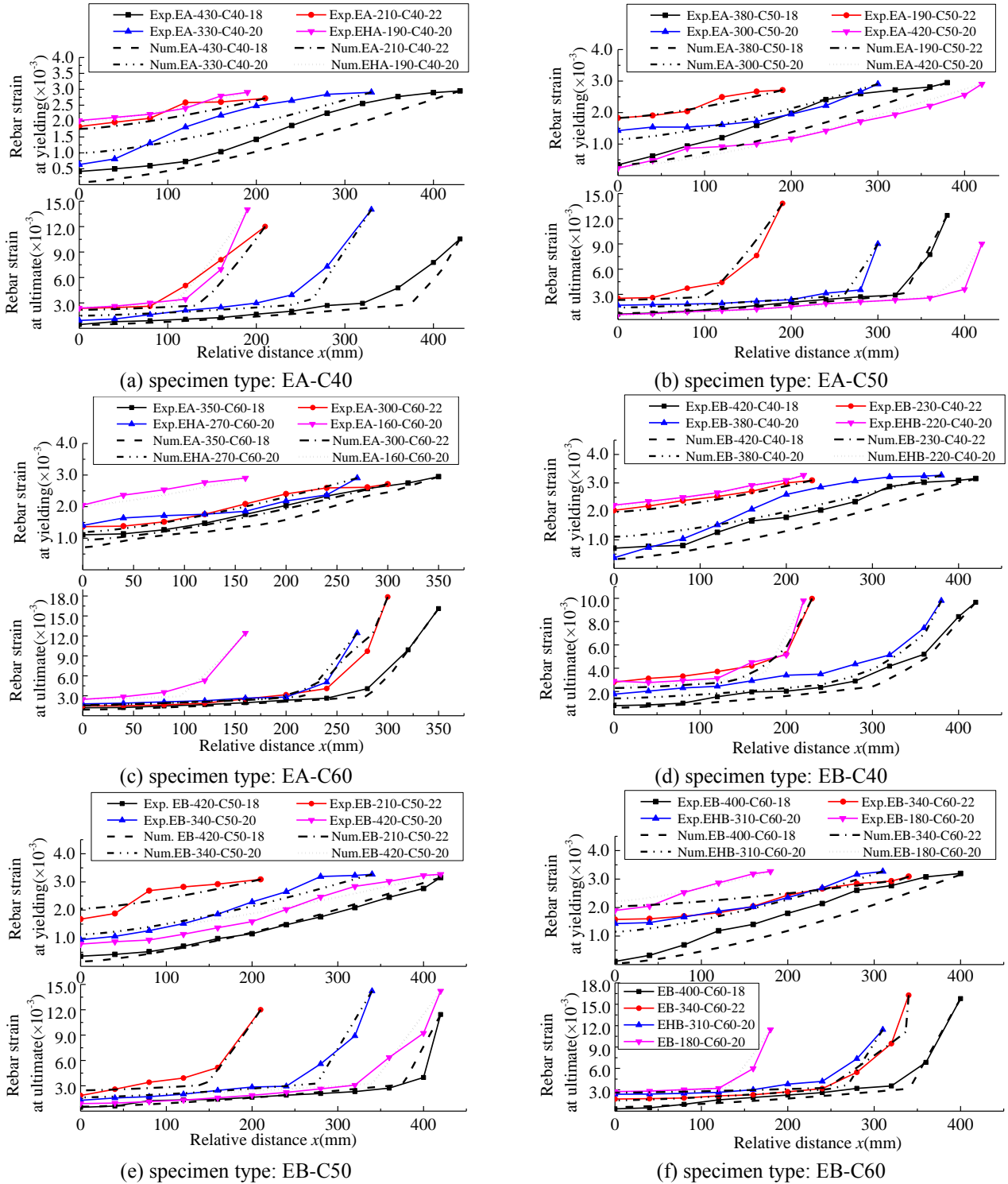


Fig.13 Comparisons between the experimental and numerical results of the rebar strain distribution in the exterior beam-column connections at the yielding and ultimate states

#### 4. Experimental and numerical results

During the loading process, all the test specimens experienced three characteristic states, namely appearance of the first major cracks, the yielding state when tensile reinforcement at the critical section reached yielding, and finally, the ultimate limit state when concrete strain in the

extreme compressed fibres of the critical section reached ultimate strain. The loads in each characteristic state obtained from the experimental results were compared with the numerical results, as shown in Fig.11.

Strain distribution of the anchorage reinforcement in the test specimens at the yielding and ultimate states was obtained from strain-gauge measurements, as shown in

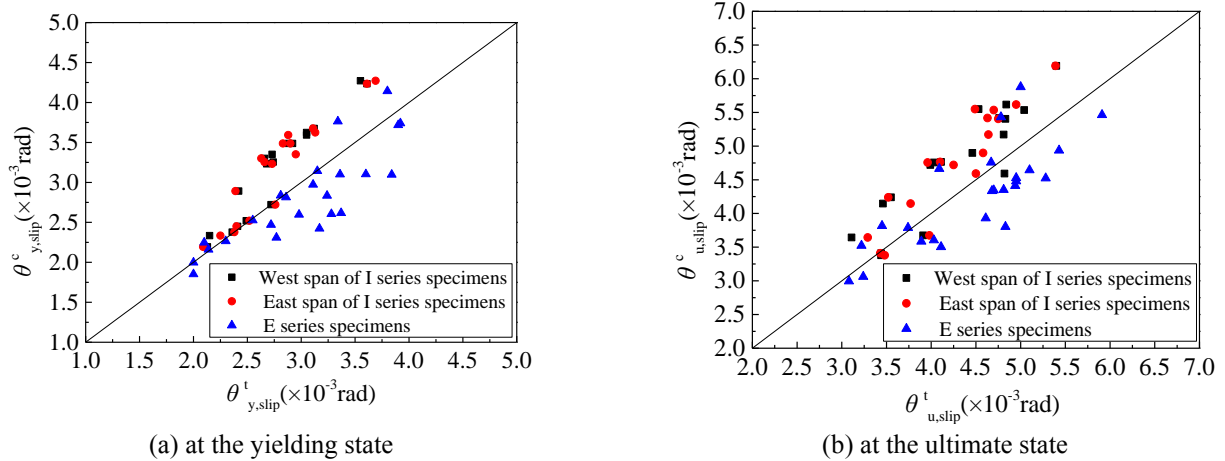


Fig. 14 Comparison of the experimental additional fixed-end rotations with numerical calculations

Table 4 Parameters of numerical specimens

Conditions	Specimens No.	$f_y$ (MPa)	$f_c$ (MPa)	$d_b$ (mm)	$c/d$	$l_{ah}$ (mm)
1	FY1	400				
	FY2	500				
	IA-400-C40-18	590	40.00	18	0.20	200
	IB-400-C40-18	631				
	FY3	700				
2	FY4	400				
	FY5	500				
	IA-600-C50-20	580	47.20	20	0.15	300
	IB-600-C50-20	654				
	FY6	700				
3	FY7	400				
	FY8	500				
	FY9	550	59.80	22	0.13	400
	IB-800-C60-22	618				
	FY10	700				
4	FC1		30.00			
	FC2		40.00			
	IA-400-C50-18	590	47.20	18	0.16	200
	FC3		60.00			
	FC4		70.00			
5	FC5		30.00			
	IB-600-C40-20		40.00			
	FC6	654	50.00	20	0.17	300
	FC7		60.00			
	FC8		70.00			
6	FC9		30.00			
	FC10		40.00			
	FC11	543	50.00	22	0.18	400
	IA-800-C60-22		59.86			
	FC12		70.00			

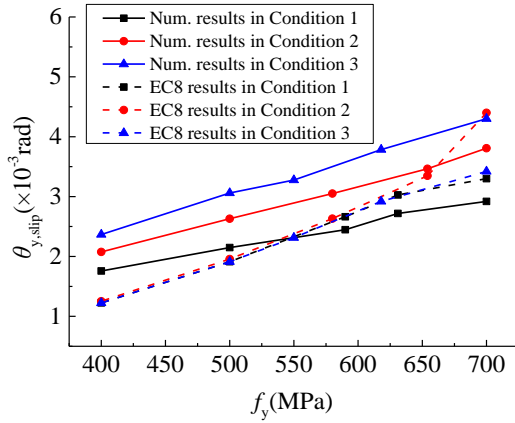
Figs. 12-13. As shown in Fig. 3, the origin of the abscissa in Fig.12 represents the midpoint of the straight steel bar through the interior beam-column connection and the one in Fig. 13 represents the start point of the straight anchorage length in the exterior connection. It can be seen that the rebar strain gradually decreased from the critical section to the co-ordinate origin, which may be attributed to the bond stress between the reinforcement and concrete. This demonstrates the occurrence of strain penetration in

beam-column connection and consequently slip. At the ultimate state, the rebar strain declined sharply until reaching the yield strain point. Strain distribution of the anchorage reinforcement obtained from the numerical study is presented in Figs. 12-13 for comparison and these results are observed to be consistent with the experimental results.

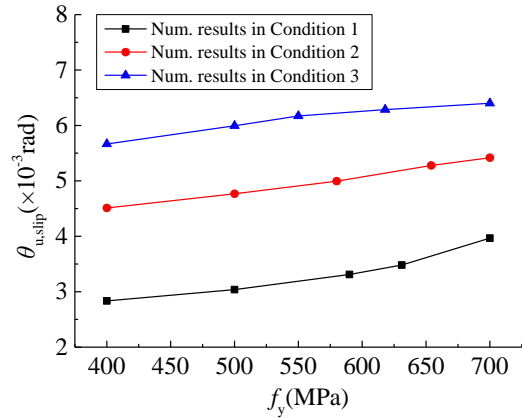
Based on the tensile strain distribution of the anchorage reinforcement, additional fixed-end rotation at the yielding and ultimate states can be calculated by combining Eqs.

Table 4 (continued)

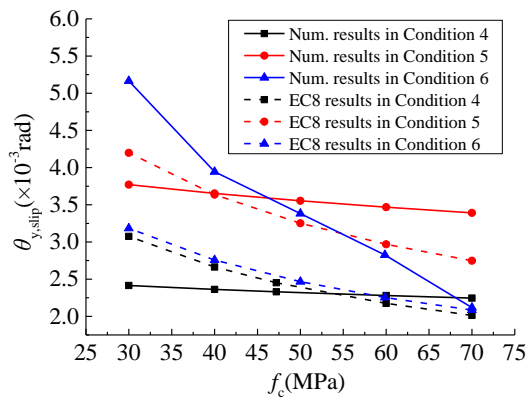
	DB1			14		156
	DB2			16		178
7	IB-400-C60-18	631	62.30	18	0.13	200
	DB3			20		222
	DB4			22		244
	DB5			25		278
	DB6			14		255
	DB7			16		291
8	DB8	618	47.20	18	0.17	327
	DB9			20		364
	IB-800-C50-22			22		400
	DB10			25		455
	DB11			14		210
	DB12			16		240
9	DB13	581	40.00	18	0.16	270
	IA-600-C40-20			20		300
	DB14			22		330
	DB15			25		375
	CD1				0.10	
10	IB-400-C50-18	631	47.20	18	0.18	200
	CD2				0.25	
	CD3				0.30	
	CD4				0.10	
11	IB-800-C40-22	618	44.88	22	0.18	400
	CD5				0.25	
	CD6				0.30	
	CD7				0.10	
12	IB-600-C60-20	654	60.70	20	0.17	300
	CD8				0.25	
	CD9				0.30	
	LAH1					144
	IA-400-C60-18					200
	LAH2					216
	LAH3					270
13	LAH4	590	62.30	18	0.12	324
	LAH5					360
	LAH6					396
	LAH7					450
	LAH8					540
	LAH9					160
	LAH10					200
	LAH11					240
14	IA-600-C50-20	581	47.20	20	0.20	300
	LAH12					360
	LAH13					400
	LAH14					440
	LAH15					500
	LAH16					600
	LAH17					176
	LAH18					220
	LAH19					264
	LAH20					330
15	IA-800-C40-22	543	44.80	22	0.16	400
	LAH21					440
	LAH22					484
	LAH23					550
	LAH24					660



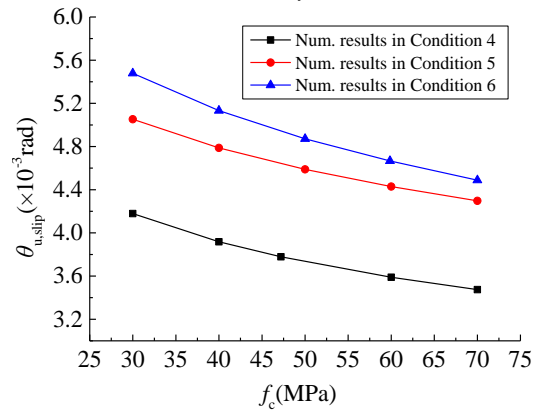
(a) at the yielding state



(b) at the ultimate state

Fig. 15 Variation in additional fixed-end rotation with respect to  $f_y$ 

(a) at the yielding state



(b) at the ultimate state

Fig. 16 Variation in additional fixed-end rotation with respect to  $f_c$ 

(11)-(12). A comparison between numerical results corresponding to additional fixed-end rotation due to strain penetration and the test results is shown in Fig. 14. It indicates good agreement between the two sets.

## 5. Parametric study

Due to limited number of test specimens, a systematic parametric study was carried out based on the numerical analysis program to investigate the influence of the key factors on additional fixed-end rotations at the yielding and ultimate states. The parameters included the yield strength of steel bar  $f_y$ , concrete compressive strength  $f_c$ , diameter  $d_b$  and anchorage length  $l_{ah}$  of steel bar in beam-column connections, as well as the ratio of neutral axis depth to section effective depth  $c/d$ . 87 specimens were designed and the details of these specimens are listed in Table 4. The values of the parameters are based on the test specimens in this study. Fifteen conditions were categorized according to the variables studied. In each condition, when one parameter was studied, other parameters were kept constant.

In Eurocode 8: Part 3 (2005), the fixed-end rotations at the yielding state  $\theta_{y,slip}$  is obtained using the simplified local bond-slip relationship  $\tau_{be} = \sqrt{f_c}$ , as given in Eq. (16)

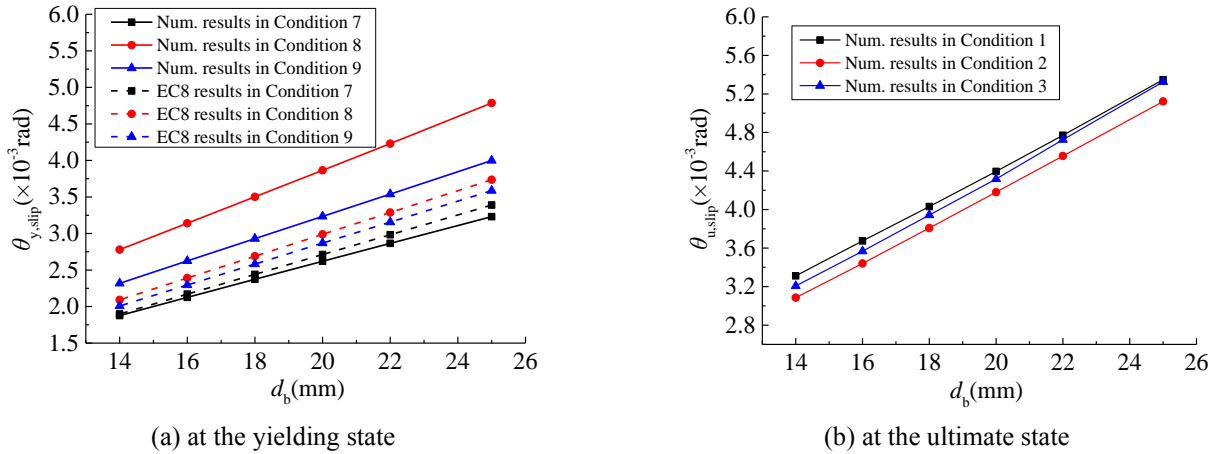
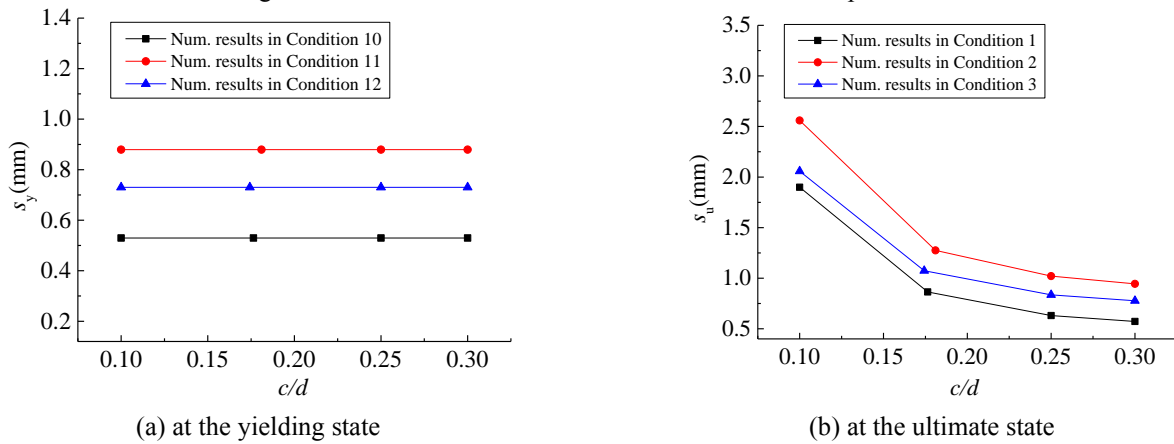
$$\theta_{y,slip} = \frac{\varepsilon_y}{d-d'} \frac{d_b f_y}{6\sqrt{f_c}} \quad (16)$$

where  $d-d'$  is the distance between tension and compression reinforcement. In the parametric study of fixed-end rotations at the yielding state, Eq. (16) was also used for comparison. The empirical formula at the ultimate state was not used because the definitions of ultimate state varied between different reports.

### 5.1 Effect of $f_y$

The yield strength of steel bars  $f_y$  is considered to be a main factor that affects additional fixed-end rotation due to strain penetration. The specimens for numerical analysis in Conditions 1-3 were selected to study the relationship between additional fixed-end rotation and  $f_y$  at the yielding and ultimate states, as shown in Fig. 15. As  $f_y$  increases from 400 to 700 MPa, an approximately linear increase can be observed in  $\theta_{y,slip}$  and  $\theta_{u,slip}$ . The increase in  $f_y$  accelerates bond failure between the reinforcement and concrete and in turn improves strain penetration, thus leading to an increase in additional fixed-end rotation.

A comparison between Fig. 15(a) and Fig. 15(b) shows that the slopes of the trendlines in the former are greater than those in the latter. This implies that the growth rate of


 Fig. 17 Variation in additional fixed-end rotation with respect to  $d_b$ 

 Fig. 18 Variation in slippage at beam-column interface with respect to  $c/d$ 

$\theta_{y,slip}$  is faster than that of  $\theta_{u,slip}$  with respect to an increase in  $f_y$ . As a result, the influence of strain penetration on additional fixed-end rotation at the early stages before yielding should be given special attention when high-strength steel bars are used as tensile reinforcement in beam-column connections.

Furthermore, comparing the predictions of  $\theta_{y,slip}$  based on EC8 with the numerical results in Fig. 15(a), it can be seen that in some cases EC8 specifications slightly underestimate fixed-end rotations at the yielding state.

### 5.2 Effect of $f_c$

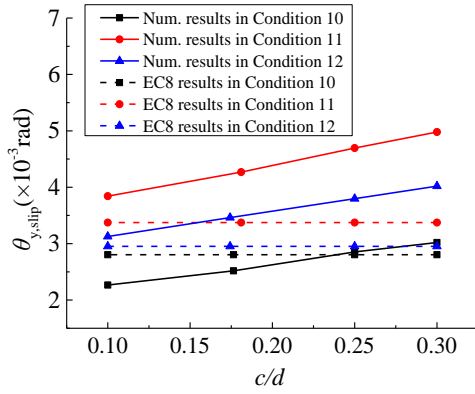
Strain penetration of the reinforcement in a beam-column connection is closely related to bond stress between the reinforcement and concrete. From the bond stress-slip relationship (Fig. 6), it can be understood that the concrete compressive strength  $f_c$  plays a major role in the change of the bond stress. Based on the numerical results of the specimens corresponding to Conditions 4-6, Figs. 16(a)-16(b) show a clear decreasing trend in  $\theta_{y,slip}$  and  $\theta_{u,slip}$  when  $f_c$  varies from 30 to 70 MPa. An increase in  $f_c$  strengthens the bond between the reinforcement and concrete, and consequently, results in a faster decline in rebar strain along the anchorage length, which reduces the ability of strain penetration. Therefore, an increase in  $f_c$  is unfavourable for additional fixed-end rotation.

### 5.3 Effect of $d_b$

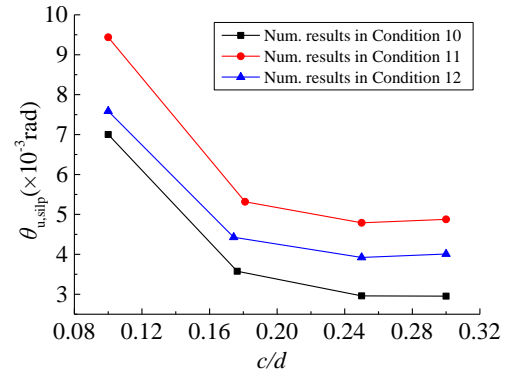
The diameter of steel bars  $d_b$  is another factor that is believed to influence the bond resistance between reinforcement and concrete. Consider the case in which a reinforcing bar with a diameter  $d_b$  is anchored in concrete and a tensile force is applied at the loading end. The tensile force is balanced by the bond resistance surrounding the steel bar. At a constant tensile force, an increase in  $d_b$  leads to an increase in the bond surface area, which in turn reduces the bond resistance. As a result, rebar stress reduces slowly along the anchorage length. This implies that an increase in  $d_b$  increases the extent of yield penetration and is advantageous for additional fixed-end rotation. This trend is accurately reflected by the numerical parametric study corresponding to Conditions 7-9, as shown in Figs. 17(a)-17(b). As  $d_b$  increased from 14 to 25 mm,  $\theta_{y,slip}$  and  $\theta_{u,slip}$  increased by averages of 72.2% and 62.7%, respectively. This indicates that  $d_b$  has a significant effect on the strain penetration of the reinforcement and similar trends were obtained from the predictions of  $\theta_{y,slip}$  based on EC8.

### 5.4 Effect of $c/d$

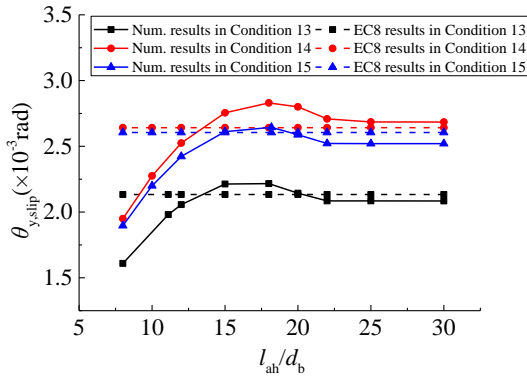
The ratio of neutral axis depth to section effective depth  $c/d$  is a complicated factor affecting additional fixed-end rotation in that it has an impact on both the tensile zone



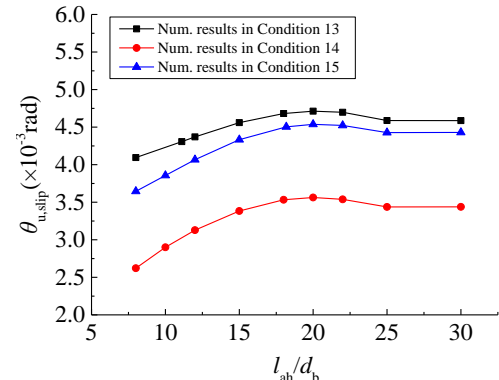
(a) at the yielding state



(b) at the ultimate state

Fig. 19 Variation in additional fixed-end rotation with respect to  $c/d$ 

(a) at the yielding state



(b) at the ultimate state

Fig. 20 Variation in additional fixed-end rotation with respect to  $l_{ah}/d_b$ 

depth of the critical section and the slip of reinforcement. It is simple to understand that the depth of the tensile zone decreases with an increase in  $c/d$  at the yielding and ultimate states. Herein, we focused on the variation in slip with  $c/d$ . The specimens with  $c/d$  in the range of 0.1~0.3 in Conditions 10-12 were analyzed.

At the yielding state, the relationship between the slip of the reinforcement at the beam-column interface  $s_y$  and  $c/d$  is shown in Fig. 18(a). It can be seen that  $s_y$  is largely constant in each condition for  $c/d$  varying from 0.1 to 0.3. This means that the influence of  $c/d$  on  $s_y$  is minimal. Based on Eq. (15), regarding the influence of  $c/d$  on the depth of the tensile zone, we know that an increase in  $c/d$  can increase  $\theta_{y,slip}$  as depicted in Fig. 19(a). However, the predictions of  $\theta_{y,slip}$  based on EC8 are almost constant as the variation in tensile zone depth with  $c/d$  at the yielding state is ignored.

At the ultimate limit state, a reduction is observed in the slip of reinforcement  $s_u$  with an increase in  $c/d$ , as shown in Fig. 18(b). The slip is obtained by integrating strain that gradually decreases along the anchorage length; meanwhile, the strain at the critical section  $\varepsilon_{su}$  is the maximum. Under the same bond conditions,  $\varepsilon_{su}$  is regarded to be positively related to slip. Moreover, rebar strain at the critical section decreases with an increase in  $c/d$  according to the equilibrium equation for the cross section. Thus, an increase in  $c/d$  leads to a reduction in  $s_u$ , which is unfavourable for  $\theta_{u,slip}$ . As shown in Fig. 19(b),  $\theta_{u,slip}$  decreases with an increase in  $c/d$ . This can be interpreted as an increase in  $c/d$

exerts greater influence on the decrease in  $s_u$  than the decrease in the depth of the tensile zone.

### 5.5 Effect of $l_{ah}/d_b$

The straight anchorage length of the reinforcement in the beam-column connection  $l_{ah}/d_b$  is rarely included in the existing formulas of additional fixed-end rotation due to strain penetration. As shown in Fig. 20(a), for the specimens in Conditions 13-15, the variation of  $l_{ah}/d_b$  has no effect on the prediction of  $\theta_{y,slip}$  by EC8. However, from the numerical study shown in Fig. 20(a),  $\theta_{y,slip}$  and  $\theta_{u,slip}$  were observed to increase when  $l_{ah}/d_b$  increased from 8 to 20. When  $l_{ah}/d_b$  is greater than 20, the additional rotations were almost constant.

Theoretically, when the anchorage length of the reinforcement in a beam-column connection is long enough, rebar strain will decrease from the maximum at the beam-column interface to zero at the unloaded end along the development length. The redundant embedment length, which is greater than the development length, is invalid for the reinforcement slip. In fact, in practical design, the straight embedded length is usually not greater than the development length. In these cases, the unloaded end is stressed. Rebar strains near the unloaded end also contribute to reinforcement slip at the beam-column interface. It can be known from Eq. (14) that an increase in  $l_{ah}/d_b$  enlarges the upper limit of strain integration and consequently increases the additional fixed-end rotation.

In many cases, hooked bars are required in beam-column connections because the straight anchorage length may not be satisfied. Hook displacement occurs if the straight lead length of the bar is not sufficient. It contributes to reinforcement slip at the beam-column interface as well. The slippage of hooked bars in tension was studied by Soroushian *et al.* experimentally in 1988. Seven specimens were tested to simulate the behaviour of hooked bars anchored in an exterior beam-column connection and subjected to pullout forces. It was reported that hook behaviour was related to the diameter of the anchored bars, confinement of the joint, and the compressive strength of concrete. Based on the experimental results, a model was proposed for the relationship between the force resisted by the hook and hook displacement, as shown in Fig. 21, and the relevant mathematical expressions were as follows:

$$P_h = P_{hu} \left( \frac{\delta_h}{2.54} \right)^{0.2} \quad (17)$$

$$P_{hu} = 271(0.05d_b - 0.25) \quad (18)$$

$$P_{hf} = 0.54P_{hu} \quad (19)$$

where  $P_h$  is the hooked force,  $\delta_h$  is the hooked displacement,  $d_b$  is the diameter of the hooked bars, and  $P_{hu}$  and  $P_{hf}$  are the maximum values and residual values of the hooked forces, respectively, as depicted in Fig. 21.

Based on the above model for hook displacement proposed by Soroushian (1988), the relationship between the ratio of hook displacement  $\delta_h$  to slippage  $s$  and  $l_{ah}/d_b$  at the yielding and ultimate states was obtained, as shown in Fig.22. It can be seen that  $\delta_h$  decreases with the increase of  $l_{ah}/d_b$  and tends to approach zero when  $l_{ah}/d_b$  is greater than

20. This indicates that the hook displacement makes little contribution to additional fixed-end rotation when  $l_{ah}/d$  is greater than 20. In summary, increasing  $l_{ah}/d_b$  within a certain range is beneficial for increasing the additional fixed-end rotation.

### 6. Conclusion

In this study, 42 RC beam-column connections with different design parameters were tested under a monotonic load. In addition, a numerical analysis program was conducted to study the strain penetration of reinforcement in the test specimens. A total of 87 specimens were designed for numerical analysis to investigate the factors influencing the strain penetration effect. The main conclusions can be summarised as follows:

- According to the experimental results on beam-column connections with different parameters under monotonic loading, the additional fixed-end rotation at the ultimate state was 1.26~1.89 times greater than that at the yielding state. Moreover, there was good consistency between the numerical and test results.
- Comparisons with the results of numerical analysis indicate that the specifications in EC8 slightly underestimate additional fixed-end rotations at the yielding state by an average of 14.97%.
- As the yield strength of reinforcement  $f_y$  increased

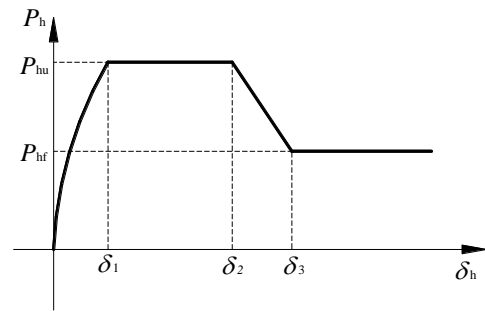
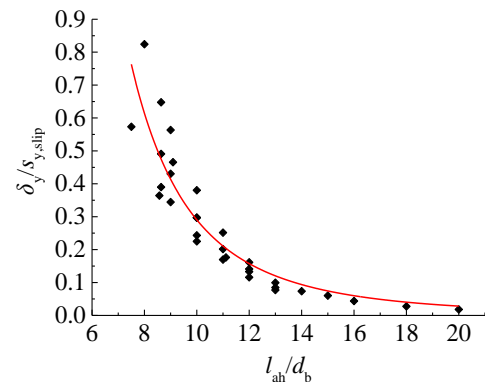
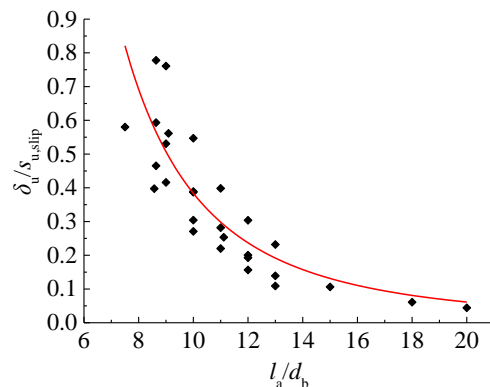


Fig. 21 Hook force–hook deformation relationship



(a) at the yielding state



(b) at the ultimate state

Fig. 22 Variation in  $\delta_h/s_{slip}$  with respect to  $l_a/d_b$

from 400 to 700 MPa, additional fixed-end rotation at the yielding and ultimate states increased by averages of 76.67% and 32.97%, respectively. This indicates that strain penetration effects at the early stages before yielding should be given special attention when high-strength steel bars are used as tensile reinforcement in beam-column connections.

- Concrete compression strength  $f_c$  and diameter of the reinforcement  $d_b$  potentially affect the bond between the reinforcement and concrete, thus influencing strain penetration of the anchorage steel bars in beam-column connections. According to numerical analysis, the additional fixed-end rotation increases with a decrease in  $f_c$  and an increase in  $d_b$ .
- For both straight and hooked steel bars, increasing the relative straight lead anchorage length  $l_{ah}/d_b$  within a certain range is beneficial for increasing additional fixed-end rotation. An increase in  $\theta_{y,slip}$  and  $\theta_{u,slip}$  is obtained when  $l_a/d$  increases from 8 to 20. When  $l_a/d$  is greater than 20, the additional rotations remained constant.

- As the ratio of neutral axis depth to section effective depth  $c/d$  varied from 0.1–0.3, a slight increase in the numerical results of  $\theta_{y,slip}$  was observed, while  $\theta_{u,slip}$  decreased, especially when  $c/d$  was smaller than 0.2.

## Acknowledgments

Support for this research from the National Natural Science Foundation of China (NSFC, Grant No. 51378146) is gratefully acknowledged.

## References

- Alva, G.M.S. (2013), “Moment–rotation relationship of RC beam–column connections: Experimental tests and analytical model”, *Eng. Struct.*, **56**(6), 1427–1438. <https://doi.org/10.1016/j.engstruct.2013.07.016>.
- CEB-FIP (2010), CEB-FIB Model Code International Federation for Structural Concrete (fib), Committee Eurointernational Du Beton, Thomas Telford Services Ltd., London, United Kingdom.
- EC8 (2005), Design provisions of structures for earthquake resistance -Part 3: Assessment and retrofitting of buildings, CEN, Brussels, Belgium.
- Fisher, Matthew J., and H. Sezen. (2011), “Behavior of exterior reinforced concrete beam–column joints including a new reinforcement”, *Struct. Eng. Mech.*, **40**(6), 27–37. <https://doi.org/10.12989/sem.2011.40.6.867>.
- GB 50010-2010 (2010), Code for design of concrete structures, Architecture and Building Press; Beijing, China. (in Chinese).
- Giuseppe Campione, Francesco Cannella, Liborio Cavaleri and Alessia Monaco. (2018), “Simplified analytical model for flexural response of external R.C. frames with smooth rebars”, *Struct. Eng. Mech.*, **66**(4), 531–542. <https://doi.org/10.12989/sem.2018.66.4.531>.
- Mergos, P.E. (2013), “The anchorage–slip effect on direct displacement-based design of R/C bridge piers for limiting material strains”, *Comput. Concrete*, **11**(6), 493–513. <https://doi.org/10.12989/cac.2013.11.6.493>.
- Mergos, P.E. and Kappos, A.J. (2012), “A gradual spread inelasticity model for R/C beam–columns accounting for flexure shear and anchorage slip”, *Eng. Struct.*, **44**(6), 94–106. <https://doi.org/10.1016/j.engstruct.2012.05.035>.
- Mergos, P.E. and Kappos, A.J. (2016), “Estimating fixed-end rotations of reinforced concrete members at yielding and ultimate”, *Struct. Concrete*, **16**(4), 537–545. <https://doi.org/10.1002/suco.201400067>.
- Monti, G., Filippou, F.C. and Spacone, E. (1997), “Analysis of hysteretic behavior of anchored reinforcing bars”, *ACI Struct. J.*, **94**(2), 248–261.
- Panagiotakos, T.B. and Fardis M.N. (2001), “Deformations of reinforced concrete members at yielding and ultimate”, *ACI Struct. J.*, **98**, 135–148.
- Park, G.K., Kwak, H.G. and Filippou, F.C. (2017), “Blast Analysis of RC Beams Based on Moment–Curvature Relationship Considering Fixed–End Rotation”, *J. Struct. Eng.*, **143**(9), [https://doi.org/10.1061/\(ASCE\)ST.1943-541X.0001837](https://doi.org/10.1061/(ASCE)ST.1943-541X.0001837).
- Paulay, T. and M.J.N. Priestley. (1992), *Seismic Design of Reinforced Concrete and Masonry Buildings*, John Wiley and Sons, New York, NY, USA.
- Pimanmas, A., and Thai, D.X. (2011). “Response of lap splice of reinforcing bars confined by FRP wrapping: application to nonlinear analysis of RC column”, *Struct. Eng. Mech.*, **37**(37), 111–129. <https://doi.org/10.12989/sem.2011.37.1.095>.
- Rajagopal, S., and S. Prabavathy. (2013), “Study of exterior beam–column joint with different joint core and anchorage details under reversal loading”, *Struct. Eng. Mech.*, **46**(6), 809–825. <https://doi.org/10.12989/sem.2013.46.6.809>.
- Saatcioglu, M., Alsiwat, J.M. and Ozcebe, G. (1992), “Hysteretic Behavior of Anchorage Slip in R/C Members”, *J. Struct. Eng.*, **118**(9), 2439–2458. [https://doi.org/10.1061/\(ASCE\)0733-9445\(1992\)118:9\(2439\)](https://doi.org/10.1061/(ASCE)0733-9445(1992)118:9(2439)).
- Sarti, F., Palermo, A. and Pampanin, S. (2016), “Experimental calibration of parallel-to-grain strain penetration length for internal epoxyed bars”, *Construct. Build. Mater.*, **112**, 970–979. <https://doi.org/10.1016/j.conbuildmat.2016.03.009>.
- Sezen, H. and Moehle, J. (2003), “Bond–slip behaviour of reinforced concrete members”, *fib Symposium Concrete Structures in Seismic Regions*, Athens, Greece, May.
- Soroushian, P., Obaseki, K., Nagi, M. and Rojas, M. (1988), “Pullout behavior of hooked bars in exterior beam–column connections”, *ACI Struct. J.*, **85**, 269–276.
- Youlin, X., Wendu, S. and Hong, W. (1994), “An experimental study of bond–anchorage properties of bars in concrete”, *J. Build. Struct.*, **3**, 26–37.

CC